ACS Biomaterials SCIENCE & ENGINEERING

Article

pubs.acs.org/journal/abseba

Protein−Nanoparticle Hydrogels That Self-assemble in Response to Peptide-Based Molecular Recognition

Andreina Parisi-Amon,[†] David D. Lo,[‡] Daniel T. Montoro,[‡] Ruby E. Dewi,[§] Michael T. Longaker,[‡] and Sarah C. Heilshorn*[,§]

[†]Bioengineering, Stanford University, Stanford, California 94305, United States

[‡]Stanford Medical School, Stanford University, Stanford, California 94305, United States

[§]Materials Science and Engineering, Stanford University, 476 Lomita Mall, McCullough 246, Stanford, California 94305, United States

Supporting Information

ABSTRACT: Recently, supramolecular hydrogels assembled through nonspecific interactions between polymers and nanoparticles (termed PNP systems) were reported to have rapid shear-thinning and self-healing properties amenable for cell-delivery applications in regenerative medicine. Here, we introduce protein engineering concepts into the design of a new family of PNP hydrogels to enable direct control over the polymer−nanoparticle interactions using peptide-based molecular recognition motifs. Specifically, we have designed a bifunctional peptide that induces supramolecular hydrogel assembly between hydroxy apatite nanoparticles and an engineered, recombinant protein. We demonstrate that this supramolecular assembly critically requires molecular recognition, as no assembly is observed in the presence of control peptides with a scrambled amino acid sequence. Titration of the bifunctional peptide enables direct control over the number of physical cross-links within the system and hence the resulting hydrogel mechanical properties. As with previous PNP systems, these materials are rapidly shear-thinning and self-healing. As proof-of-concept, we demonstrate that these materials are suitable for therapeutic cell delivery applications in a preclinical murine calvarial defect model.

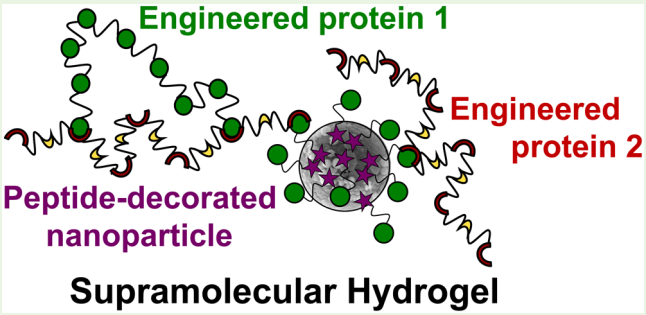

KEYWORDS: *hydrogel, protein engineering, hydroxy apatite, stem cells, supramolecular assembly*

INTRODUCTION

Supramolecular hydrogels formed through noncovalent interactions have become increasingly used in regenerative medicine applications since they enable encapsulation of cells without exposure to chemical cross-linking reagents.[1,2] Furthermore, due to the reversible nature of noncovalent interactions, these supramolecular hydrogels are shear-thinning and self-healing.[3,4] This on-demand injectability makes supramolecular hydrogels easy to use in a clinical setting compared to covalently cross-linked hydrogels, where the kinetics of the cross-linking reaction must be carefully timed to coincide with material delivery.[4]

A new class of supramolecular hydrogels is polymer−nanoparticle (PNP) materials that rely on nonspecific interactions to adsorb polymer chains onto the surfaces of colloidal particles, thereby forming an interconnected network.[5,6] Here, we introduce protein engineering concepts into the design of a new family of PNP hydrogels that enable direct control over the polymer−nanoparticle interactions using peptide-based molecular recognition motifs. Specifically, nanoparticles were "decorated" with multiple copies of an engineered, bifunctional peptide, which allowed physical cross-linking with a recombinantly engineered protein to form a supramolecular hydrogel (Figure 1). This peptide-based molecular recognition strategy enables direct control over the number of peptide−nanoparticle interactions and hence the number of physical cross-links and the resulting stiffness of the hydrogel material. As proof-of-concept, we demonstrate that these materials are suitable for therapeutic delivery of adipose-derived stem cells (ASCs) for bone regeneration.

Bones are complex mineralized tissues, comprising a mineral phase interfaced at the molecular level with an organic matrix. The current gold standard treatment for nonhealing skeletal defects is autologous bone grafts, despite the inherent risk of the invasive surgery and associated donor-site morbidity.[7−9] When patients are able to provide sufficient autologous bone tissue and tolerate the additional surgery, this treatment is highly successful. When autografts are not feasible, synthetic

Special Issue: Designer Protein Biomaterials

Received: May 26, 2016
Accepted: August 8, 2016

ACS Publications © XXXX American Chemical Society

DOI: 10.1021/acsbiomaterials.6b00286
ACS Biomater. Sci. Eng. XXXX, XXX, XXX−XXX

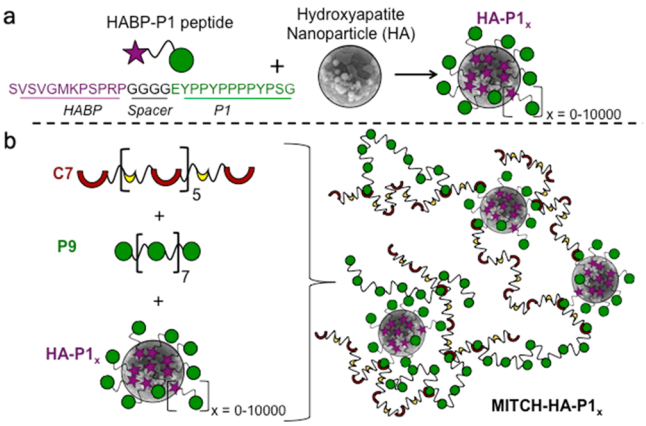

Figure 1. Schematic of protein-engineered, polymer−nanoparticle hydrogel with specific molecular recognition. (a) Binding of HABP-P1 peptides to hydroxyapatite nanoparticles creates HA-P1$_x$, where x is the number of peptides per HA particle in solution. (b) Mixing of HA-P1$_x$ with the recombinant proteins P9 and C7 induces supramolecular assembly of the MITCH-HA-P1$_x$ hydrogel with direct molecular linkage between the inorganic and organic phases.

materials are substituted; however, these suffer from much lower success rates.[8]

Treatments harnessing the regenerative potential of adult stem cells, such as ASCs, are an increasingly promising alternative to autologous bone grafts. This strategy has the advantage of being less invasive than traditional bone harvesting procedures, while retaining the immunological benefits of using a patient's own cells. These cells are typically incorporated within scaffolds before transplantation, both to keep the cells localized to the site of delivery and to create the appropriate regenerative microenvironment within the injury site.[10,11] Unfortunately, widespread implementation of these treatments is challenging in the near term, given the current need for *ex vivo* cell expansion and cell-scaffold integration prior to implantation. These laborious and costly protocols require advanced tissue culture facilities and expertise, which are not standard in most hospital settings.[7,10]

Our goal is to create a PNP material enabling on-demand encapsulation of regenerative adult stem cells for immediate surgical use in the form of an easily transplantable cell-scaffold construct. To be clinically translatable for bone regeneration applications, this material must stimulate osteogenesis *in vivo*, while eliminating the costly and time-consuming need to culture harvested adult stem cells. Toward this goal, we have developed an osteoconductive material, MITCH-HA-P1$_x$, that integrates hydroxy apatite nanoparticles within a supra-molecular, protein-engineered hydrogel (Figure 1a,b). This protein−nanoparticle hydrogel acts as an on-demand cell carrier, gently encapsulating ASCs and immobilizing them within a porous scaffold for immediate implantation into critically sized defect sites without any *ex vivo* tissue culture steps. Once implanted, the hydroxy apatite nanoparticles provide osteoconductive cues to assist the ASCs in promoting bone regeneration.

■ MATERIALS AND METHODS

Synthesis of MITCH-HA-P1$_x$ Components. The full amino acid sequences of all recombinant proteins and synthetic peptides used are available in Supporting Information, Table S1. Engineered proteins C7 and P9 were cloned, synthesized, and purified as previously reported.[12] Briefly, DNA sequences of C7 and P9 proteins were cloned into the pET15b (Novagen) and pJExpress 414 (DNA 2.0) vectors, respectively, and transformed into BL21(DE3)pLysS *Escherichia coli* expression strain (Invitrogen). Recombinant proteins were expressed following induction with 0.5 mM isopropyl β-D-1-thiogalactopyranoside (IPTG) and purified via binding of terminal polyhistidine tags to Ni-nitrilotriacetate resin (Qiagen). Purified C7 was buffer exchanged and concentrated in saline by centrifugation across 10-kDa Amicon Ultracel-10K filter units (Millipore). Purified P9 was dialyzed into water, lyophilized, and reconstituted in saline. Protein identity and purity were confirmed by gel electrophoresis and Western blotting. As previously determined by isothermal titration calorimetry, the C and P domains bind together with a 1:1 stoichiometry with an apparent dissociation constant, K_d, of 4.6 ± 0.01 μM within the context of our engineered biomaterial.[12] HABP-P1 peptide was synthesized by GenScript and reconstituted according to the manufacturer's instructions. nanoHA (Sigma-Aldrich, nanopowder <200 nm) was suspended in PBS and sonicated on ice for 4 min at 50% amplitude, alternating one second on/one second off, with an ultrasonic processor (UP50H, MS1 tip, Heilscher) for full dispersion of the particles. The appropriate amount of HABP-P1 peptide was added, and the solution was inverted multiple times before incubating overnight at 4 °C while shaking to allow for binding of the peptides to the nanoHA.

Rheological Studies. Experiments were performed on an ARG2 rheometer (TA Instruments; New Castle, DE) with conical plate geometry (20 mm diameter, 1° cone angle) at 37 °C with a humidity chamber. Solutions were prepared in the barrel of a 28-gauge syringe and ejected onto the platform. Dynamic oscillatory measurements were used to characterize C7:P9 and MITCH-HA-P1$_x$ formulations via frequency sweeps from 0.01 to 100 Hz. A constant linear shear rate of 0.1 s^{-1} was applied to monitor material viscosity over time. Altering the polymer weight fraction or the ratio of C7 to P9 polymers was previously reported to result in altered hydrogel mechanical properties.[13] For all hydrogels tested in this study, the final concentration of C7 was 5 wt/vol %, and the final concentration of P9 was 5 wt/vol %, leading to an overall polymer weight fraction of 10% in the hydrogels.

mASC Isolation. All *in vivo* work were performed under protocols approved by the Stanford Administrative Panel on Laboratory Animal Care and in accordance with NIH guidelines for the care and use of laboratory animals (NIH Publication #85-23 Rev. 1985). To isolate mASCs, subcutaneous inguinal fat pads from five-week-old GFP/firefly luciferase double transgenic mice (Jackson Laboratory) were removed and washed sequentially in serially diluted betadine (Purdue Frederick Co.) and saline. Tissues were diced and digested with 0.075% Type II collagenase (SigmaAldrich) in Hank's balanced salt solution at 37 °C for 30 min in a shaking water bath. Digestion was neutralized with Dulbecco's modified Eagle's α-glutamax medium (Invitrogen) containing 10% fetal bovine serum (FBS) (Invitrogen). Neutralized cells were centrifuged at 4 °C for 10 min to separate mature adipocytes from the stromal-vascular fraction. Floating adipocytes were aspirated, and the pellet was resuspended in medium and filtered through a 100 μm strainer before being cryopreserved. Cells were cultured, but not passaged, in DMEM supplemented with 10% FBS and 100 IU/mL penicillin/streptomycin (Gibco) at 37 °C and 5% atmospheric CO_2 and trypsinized immediately before transplantation.

PLGA/HA Scaffold Preparation. Hydroxy apatite-coated PLGA scaffolds were fabricated from 85/15 poly(lactic-*co*-glycolic acid) (inherent viscosity = 0.61dL/g, Birmingham Polymers) by solvent casting and a particulate leaching process. Briefly, PLGA/chloroform solutions were mixed with 200−300 μm diameter sucrose to obtain 92% porosity (volume fraction) and compressed into thin sheets in a Teflon mold. After freeze-drying overnight, scaffolds were immersed in three changes of double-distilled (dd) H_2O to dissolve the sucrose and gently removed from the Teflon plate with a fine-tip spatula. After particulate leaching, all scaffolds were disinfected by immersion in 50%, 60%, and 70% ethanol for 30 min each, followed by three rinses of ddH_2O. All scaffolds were dried under a laminar flow hood. After scaffold fabrication, scaffolds were coated with hydroxy apatite. SBF (simulated body fluid) solution was prepared with ion concentrations that were five times that of human blood plasma. All solutions were

DOI: 10.1021/acsbiomaterials.6b00286
ACS Biomater. Sci. Eng. XXXX, XXX, XXX−XXX

sterile filtered through a 0.22 μm PES membrane (Nalgene). Immediately before the coating process, dried PLGA scaffolds were subjected to glow discharge, argon-plasma etching (Harrick Scientific) to improve wetting and coating uniformity. Etched PLGA scaffolds were then incubated in SBF at 37 °C inside a water-jacketed incubator to create the hydroxy apatite coating. Coated PLGA scaffolds were rinsed gently with sterile ddH_2O to wash away excess sodium chloride solution, dried in a laminar flow hood, and disinfected with 70% ethanol.

Cell/Hydrogel/Scaffold Construct Formation. 2.5×10^5 mASCs were integrated into a 3 mm diameter scaffold, either by overnight culture or via pre-encapsulation in MITCH-HA-P1$_x$ materials at the time of transplantation. For overnight culture, cells in a 10 μL volume were pipetted onto and allowed to wet into each PLGA/HA scaffold. Cells were allowed to adhere for 1 h followed by the addition of 190 μL of culture medium. The cell-seeded scaffolds were allowed to incubate at 37 °C overnight (∼12 h) to allow for cell attachment. For direct incorporation, cells were encapsulated in various MITCH formulations (MITHC-HA-P1$_0$, MITCH-HA-P1$_{100}$) in the barrel of a 28-gauge syringe, and a 10 μL volume was ejected onto and allowed to wet into each PLGA/HA scaffold immediately before implantation.

Cranial Defect Formation and Construct Implantation. Six-week old female athymic nude mice (Charles River Laboratories) were anesthetized with an anesthetic cocktail consisting of 7.5 mg/kg ketamine, 0.24 mg/kg acepromazine, and 1.5 mg/kg xylazine through intraperitoneal injections. The surgical site was cleaned with betadine and ethanol prior to making a midline sagittal incision in the scalp of the animal to expose the parietal bone. The pericranium was removed, and a critical-sized 3 mm circular defect was made in the nonsuture-associated parietal bone using a MultiPro Dremel drill with diamond-coated trephine circular cutter under constant irrigation. Extreme caution was taken not to disturb the underlying dura mater. After placement of the construct into the defect, the skin was sutured closed, and the animal was carefully monitored postoperatively.

Imaging Analysis. Bioluminescent imaging was performed with an IVIS imaging system (Xenogen Corp.), and data were acquired with LivingImage software (Xenogen Corp.) on day 0. During imaging, mice were anesthetized with 2% isoflurane. Reporter probe D-luciferin was administered via local subcutaneous injection at a dose of 1.5 mg/mouse. BLI images were acquired at 2 min intervals with an exposure time of 30 s. For each image acquisition, a gray scale body surface image was collected, followed by an overlay of the pseudocolored image of photon counts from active luciferase within the mouse. Image acquisition continued until all samples had reached peak intensity (∼30 min). Signal intensity for each sample was quantified as total flux (photons/sec) within a region of interest at peak intensity. MicroCT was performed on live animals postoperatively at weeks 0 and 4 using a high-resolution Siemens Inveon imaging system, while anesthetized with 2% isoflurane. 3D reconstructed images of the calvaria were examined, and the bone coverage of the defects was quantified with ImageJ software.

Histological Analysis. Calvarial tissue samples were harvested at 2 weeks following surgical implantation. The calvaria were fixed in 10% formalin (Electron Microscopy Sciences) at 4 °C overnight, then decalcified in 0.4 M EDTA in PBS (pH 7.2) at 4 °C for 2 weeks. Specimens were then serially dehydrated in graded ethanol steps, embedded in paraffin blocks, and sectioned at 8- μm thickness. Representative sections were stained with trichrome.

Statistical Analysis. All data are represented as averages with standard deviation error bars. For data sets with multiple comparison groups, statistical significance was determined using ANOVA with Tukey's posthoc test. For data sets with only two comparison groups, statistical significance was determined using Student's t test. For all statistical analysis, significance was accepted for p values less than 0.05.

RESULTS AND DISCUSSION

Design of a Molecularly Linked, Protein−Nanoparticle Hydrogel. MITCH-HA-P1$_x$ was developed to mimic the intimate, molecular contact between organic proteins and inorganic bone minerals found in native bone tissue. Hydroxy apatite (HA), a mineral chemically similar to the apatite found in bones, is osteoconductive when incorporated into or coated onto materials[7,14,15] and is increasingly considered osteoinductive.[7,14] While "osteoconduction" is used to describe materials that simply permit bone deposition onto the surface, "osteoinduction" is used to describe materials that actively promote osteogenic differentiation of immature cells.[16] Furthermore, the use of nanosized particles within composite materials has been shown to increase adhesion of bone cells, thereby enhancing osteoblast proliferation and differentiation and the ensuing biomineralization process.[17,18] This nanoscale dimension is of similar size and scale as the mineral crystals found interwoven with protein collagen fibers in native bone tissue.[15,17,19] Simply blending HA nanoparticles into polymeric matrices has been shown to improve matrix stiffness and enhance the ability of bone marrow-derived stromal cells to form bone.[20,21] While promising, these materials do not provide specific molecular linkages between the HA particles and the polymeric matrix. We hypothesized that molecularly anchoring the HA crystallites within the organic phase, thereby emulating the direct molecular contact between the inorganic and organic phases in natural bone tissue, would significantly improve the osteoconductive properties of the scaffold and eliminate the need for *ex vivo* ASC culture prior to transplantation.

To achieve this structure, we designed a hydrogel that incorporates nanoscale HA particles (nanoHA) directly into an engineered protein network via specific molecular recognition with mineral-binding peptides. Peptide sequences that specifically bind to a variety of inorganic materials including HA have been reported.[22−24] Using one of these HA-binding peptide (HABP) sequences, we designed a composite material in which the nanoHA become sites of cross-linking between adjacent chains. These noncovalent cross-links enable the material to undergo a sol−gel phase transition by simply mixing the otherwise nonself-assembling components together to induce supramolecular assembly. This mixing-induced gelation enables simple, on-demand cell encapsulation in a surgical setting without the use of chemical reagents or environmental triggers.[12,25]

Specifically, MITCH-HA-P1$_x$ is a protein-engineered hydrogel that heteroassembles via molecular recognition events between nanoHA and two recombinant proteins, the block copolymers C7 and P9. These copolymers contain seven and nine repeats of the CC43 WW domain (C) and the proline-rich peptide (P), respectively.[12] The P domains are connected by short hydrophilic spacers, while the C domains are connected by longer hydrophilic spacers that include the tripeptide RGD cell-binding domain (Table S1). The C and P domains noncovalently bind through specific interactions with a 1:1 stoichiometry.[26] The nanoHA is decorated with engineered, bifunctional HABP-P1 peptides that include an HABP fused to a single proline-rich peptide (P1) via a tetraglycine spacer for conformational flexibility. Specific binding of HABP-P1 peptides to nanoHA creates HA-P1$_x$, where x is the number of peptides per HA particle in solution (Figure 1a). Mixing the three components, HA-P1$_x$, P9, and C7, leads to the formation of the supramolecular organic−inorganic network MITCH-HA-P1$_x$ (Figure 1b).

Engineered, Peptide-Modified, Hydroxyapatite Nanoparticles Act as Hydrogel Cross-Linking Sites. As

DOI: 10.1021/acsbiomaterials.6b00286
ACS Biomater. Sci. Eng. XXXX, XXX, XXX−XXX

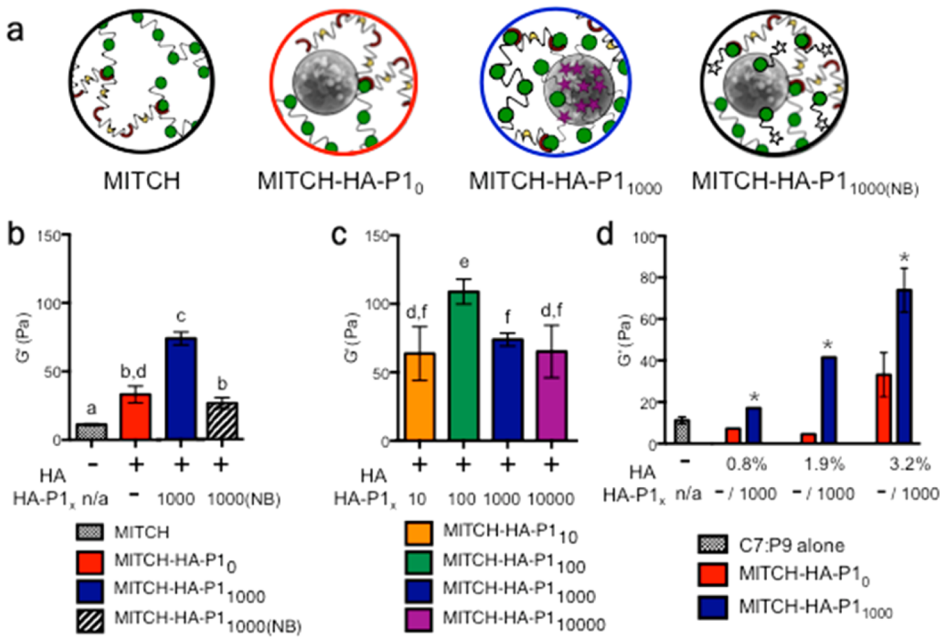

Figure 2. Hydrogel stiffness is controlled by the extent of peptide cross-linking between the HA nanoparticles and the engineered C7 protein. (a) Schematic representation of the hydrogels tested in panel b. (b) Storage modulus (G') of MITCH alone, MITCH-HA-P1$_0$ (i.e., with HA but without peptides), MITCH-HA-P1$_{1000}$ (i.e., with HA and peptides), and MITCH-HA-P1$_{1000(NB)}$ (a negative control material with a scrambled, non-HA-binding peptide). (c) Storage moduli of hydrogels with varying concentrations of HA-P1 peptide (x = 10−10,000) while maintaining a constant HA concentration of 3.2% by volume. (d) Storage moduli of hydrogels with various compositions of HA (0.8%, 1.9%, and 3.2% by volume) both without and with HABP-P1 (x = 0 and 1000, respectively). For panels b and c, statistical significance was determined using ANOVA with Tukey's posthoc test. Columns denoted with distinct lower-case letters are statistically different, with $p < 0.05$. For panel d, statistical significance was determined using Student's t test, with * denoting $p < 0.05$.

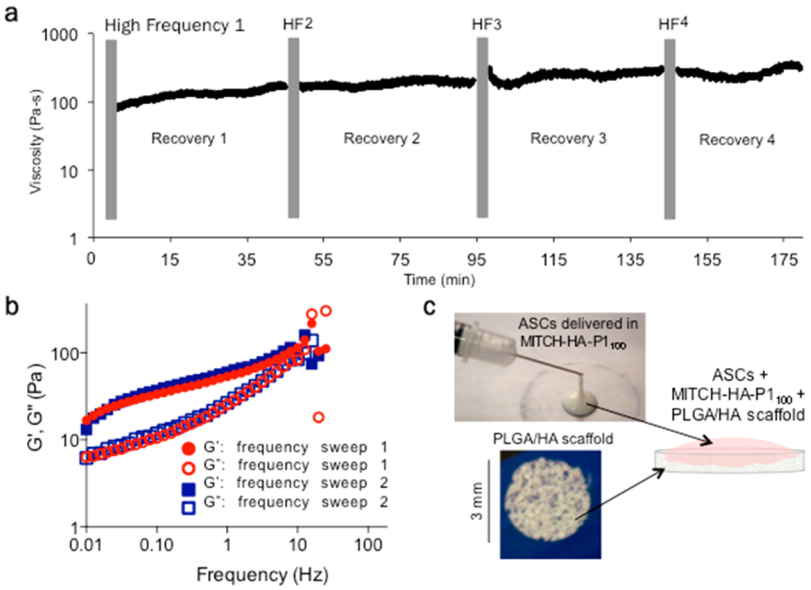

Figure 3. Shear-thinning and self-healing behavior of MITCH-HA-P1$_x$ hydrogels and their use for on-demand cell encapsulation. (a) Gel viscosity after recovery from high frequency (HF) oscillation (100 Hz) remains constant over multiple disruptions as measured by continuous shear (0.1 s^{-1}). (b) Storage (G') and loss (G'') moduli 30 min after ejection onto the rheometer specimen holder (frequency sweep 1) and after disruption by high frequency oscillation and gel recovery for 30 min (sweep 2) are similar, demonstrating full self-healing. (c) Schematic representation of a proof-of-concept application for MITCH-HA-P1$_x$ hydrogels. ASCs are pre-encapsulated within the hydrogel and delivered onto a macroporous PLGA/HA scaffold using a 28-gauge syringe needle. The hydrogel wets into the PLGA/HA scaffold and immobilizes the ASCs for immediate transplantation without *ex vivo* culture.

previously reported, the C7 and P9 copolymers alone form a mixing-induced, two-component hydrogel (termed MITCH) due to reversible association between the C and P peptide domains.[12] As expected, simply adding nanoHA to the C7 and P9 copolymers during mixing with no HABP-P1 peptide present (termed MITCH-HA-P1$_0$) significantly increased the hydrogel storage modulus (Figure 2). A volume fraction of 3.2% nanoHA caused a 2-fold increase in gel modulus

DOI: 10.1021/acsbiomaterials.6b00286
ACS Biomater. Sci. Eng. XXXX, XXX, XXX−XXX

compared to MITCH alone. However, by first decorating the nanoHA particles with HABP-P1 at x = 1000 peptides per particle to form MITCH-HA-P1$_{1000}$, the modulus was found to increase 4-fold compared to that of MITCH alone (Figure 2a,b). These data suggest that the nanoHA decorated with HABP-P1 peptide significantly increases the density of cross-links within the hydrogel network.

To confirm the specificity of the HABP-P1 peptide, a nonbinding (NB) peptide was designed by substituting four glycines for the SVSV component of the original HABP sequence, which is required for HA-specific binding,[27] and scrambling the rest of the HABP amino acid sequence (Table S1). Rheological analysis of MITCH-HA-P1$_{1000(NB)}$ found the modulus to be statistically equivalent to MITCH-HA-P1$_0$, in which no HABP-P1 is present, confirming the specific binding of nanoHA to HABP-P1 and subsequent cross-linking of HA-P1$_x$ into the composite hydrogel network (Figure 2a,b).

Additional rheological studies of the 3.2% nanoHA formulation of MITCH-HA-P1$_x$, with x = 10, 100, and 10000 found MITCH-HA-P1$_{100}$ to reach a maximal storage modulus of 108.9 Pa ± 20.2 Pa, a nearly 10-fold increase over MITCH alone (Figure 2c). This suggests that at x = 100, the nanoHA are well covered by HABP-P1 peptide, allowing them to simultaneously cross-link several different adjacent protein chains within the network. At lower levels of HABP-P1 (x = 10), fewer peptides are decorating each particle, thereby enabling fewer effective cross-links with the C7 copolymer. At higher levels of HABP-P1 (x = 1000−10000), all of the available binding sites on the nanoHA are likely occupied resulting in free HABP-P1 in solution. This results in network disruption and lower storage modulus due to competitive binding of free HABP-P1 to C sites within the C7 copolymer.

As expected, the MITCH-HA-P1$_x$ gel stiffness was directly related to the nanoHA volume fraction (Figure 2d). For a range of nanoHA volume fractions spanning 0.8%−3.2%, the stiffness of the gel was significantly increased by incorporation of the P1 peptide. These data demonstrate that both the amount of nanoHA loaded and the concentration of P1 peptide can be used to tune the final hydrogel stiffness.

The dynamic nature of the noncovalent cross-links within MITCH-HA-P1$_x$ results in shear-thinning and self-healing thixotropic properties that allow the network to disassemble and flow through a needle upon application of hand-force and to reform after force removal. The material fully recovers its initial viscosity after multiple high frequency network disruptions (i.e., shear-thinning) and recoveries (i.e., self-healing) (Figure 3a). Storage and loss moduli were also fully recovered after shear-thinning and self-healing (Figure 3b). These properties allow MITCH-HA-P1$_x$ to be used as an on-demand cell carrier, where cells can be pre-encapsulated within the gel and then delivered through a syringe needle to a porous scaffold, where the cells are entrapped by the self-healing, osteoconductive gel within the pores of the scaffold. We used this method to deliver ASCs encapsulated within MITCH-HA-P1$_{100}$ to a porous scaffold of poly(lactic-*co*-glycolic acid) coated with hydroxyapatite (PLGA/HA) (Figure 3c). Previously, these PLGA/HA scaffolds were shown to be osteogenic but only when seeded with a sufficient number of ASCs and provided with 48 h of *ex vivo* culture prior to implantation.[28,29]

Implantation of Hybrid Hydrogel/Scaffold Constructs in Critical-Size Cranial Defects. As an *in vivo* study to test the osteogenic nature of our hybrid hydrogel/scaffold constructs, we formed 3 mm, critical-size calvarial defects in the parietal bones of nude mice, which do not heal spontaneously over the lifetime of the animal (Figure 4a).[28]

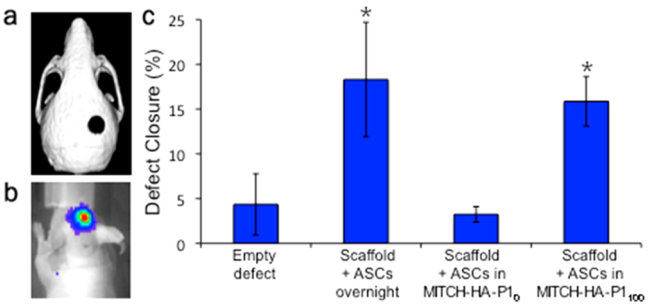

Figure 4. Preclinical model of bone regeneration. (a) A 3 mm, critical-size calvarial defect was made in the parietal bones of nude mice. (b) Six hours after ASC transplantation, successful cell delivery was confirmed by noninvasive bioluminescence imaging. (c) Comparative microCT analysis at 4 weeks was used to assess bone regeneration in the defect site. * denotes statistical significance compared to the empty defect with $p < 0.05$.

Defects were implanted with ASCs harvested from luciferase positive mice either seeded onto PLGA/HA scaffolds and cultured overnight or pre-encapsulated in MITCH-HA-P1$_{100}$ and immobilized within the PLGA/HA scaffolds via ejection from a 28-gauge syringe-needle immediately before implantation. Bioluminesence imaging, which detects metabolically active, luciferase positive ASCs, was used 6 h after surgery to confirm that viable ASCs had been transplanted into each defect site (Figure 4b). Both transplantation techniques (overnight culture of ASCs on the macroporous scaffold or pre-encapsulation of ASCs with a hydrogel to immobilize them in the macroporous scaffold immediately prior to implantation) resulted in successful delivery of viable ASCs to the defect site. *De novo* bone formation was analyzed at 4 weeks via microCT scanning, with defect bone coverage quantified from reconstructed microCT images. Controls included the defect site only with no treatment and the PLGA/HA scaffold with ASCs pre-encapsulated in MITCH-HA-P1$_0$ (i.e., the hydrogel without HABP-P1 peptide) immediately prior to implantation.

Four weeks postimplantation, animals with no treatment had minimal defect closure (<5%, Figure 4c). In contrast, animals receiving the PLGA/HA scaffold with ASCs cultured overnight or the PLGA/HA scaffold with ASCs delivered immediately prior to implantation using MITCH-HA-P1$_{100}$ demonstrated significant defect closure (>15%). Interestingly, when gels with nanoHA but without the HABP-P1 cross-linking peptide (MITCH-HA-P1$_0$) were used to deliver ASCs onto the PLGA/HA scaffold, no significant defect closure was observed compared to the untreated defect. These data suggest that the molecular-tethering strategy to incorporate nanoHA within the MITCH composite played a major role in enabling bone formation. Thus, use of the hydrogel with supramolecular structure linking the nanoHA into the protein network enabled similar levels of bone regeneration as the currently accepted protocol without requiring a period of *ex vivo* culture. To further assess the bone deposition, histological explants were analyzed 2 weeks post-transplantation (Supporting Information, Figure S1). At this early time point, scaffolds without the HABP-P1 cross-linking peptide remained largely open and porous, with minimal matrix deposition; while scaffolds with the HABP-P1 peptide demonstrate substantially more collagen

DOI: 10.1021/acsbiomaterials.6b00286
ACS Biomater. Sci. Eng. XXXX, XXX, XXX−XXX

within the scaffold at this same time point. Further study will be required to determine the mechanisms responsible for increased bone formation in the tethered nanoHA hydrogels. One possible hypothesis is that the increased stiffness of the tethered nanoHA materials leads to improved osteogenesis, as material mechanics has been shown to improve osteogenesis for bone marrow-derived mesenchymal stem cells.[30−32] For potential clinical translation, the hydrogel-enabled protocol may be simpler to implement, as it does not require the cost, expense, equipment, and expertise of a cell culture facility, and it minimizes the concerns of cell contamination that may occur when isolated cells are removed from the surgical suite.

CONCLUSIONS

Collectively, our data demonstrate that a noncovalent, molecular-recognition strategy can be used to create supramolecular hydrogels with nanoHA particles serving as cross-linking points. This work expands the repertoire of peptide functionalities that have been successfully designed into protein-engineered biomaterials and opens the door to the inclusion of other mineral-binding peptide domains. Control of the hydrogel stiffness was demonstrated by tuning either the concentration of nanoHA or the concentration of bifunctional cross-linking peptides. Because of the reversible, noncovalent cross-links within the network, the hydrogel was able to rapidly shear-thin and self-heal to regain the original rheological properties. This composite hydrogel was used to encapsulate and immobilize ASCs within a macroporous scaffold for direct implantation into a critical sized cranial defect without any prior *ex vivo* culture steps. By directly providing osteoconductive cues *in vivo*, the hydrogel/scaffold construct resulted in significant bone formation at 4 weeks, similar to that achieved by ASCs cultured on the porous scaffold overnight prior to implantation. This protocol would greatly reduce the time, cost, and risk of contamination that occur when adult stem cells are cultured *ex vivo*, thereby making the potential widespread clinical use of regenerative medicine therapies more likely.

ASSOCIATED CONTENT

Supporting Information

The Supporting Information is available free of charge on the ACS Publications website at DOI: 10.1021/acsbiomaterials.6b00286.

Amino acid sequences of all MITCH-HA-P1$_x$ components and the negative control, sequence-scrambled, nonbinding HABP peptide and histology of cranial defect implants (PDF)

AUTHOR INFORMATION

Corresponding Author

*E-mail: heilshorn@stanford.edu.

Notes

The authors declare no competing financial interest.

ACKNOWLEDGMENTS

We acknowledge funding from NIH DP2-OD-006477, Stanford Bio-X IIP4-22, NIH R01-DK-085720, NSF DMR-1508006, CIRM RT2-01938, and CIRM RT3-07948. We thank Michael T. Chung (Stanford Medical School) for providing the PLGA/HA scaffolds and Dr. Tim Doyle (Stanford Small Animal Imaging Facility) for assistance with bioluminescence imaging.

REFERENCES

(1) Appel, E. A.; Tibbitt, M. W.; Webber, M. J.; Mattix, B. A.; Veiseh, O.; Langer, R. Self-assembled hydrogels utilizing polymer−nanoparticle interactions. *Nat. Commun.* **2015**, *6*, 6295.

(2) Webber, M. J.; Appel, E. A.; Meijer, E. W.; Langer, R. Supramolecular biomaterials. *Nat. Mater.* **2016**, *15* (1), 13−26.

(3) Miao, T. X.; Fenn, S. L.; Charron, P. N.; Oldinski, R. A. Self-Healing and Thermoresponsive Dual-Cross-Linked Alginate Hydrogels Based on Supramolecular Inclusion Complexes. *Biomacromolecules* **2015**, *16* (12), 3740−3750.

(4) Pakulska, M. M.; Vulic, K.; Tam, R. Y.; Shoichet, M. S. Hybrid Crosslinked Methylcellulose Hydrogel: A Predictable and Tunable Platform for Local Drug Delivery. *Adv. Mater.* **2015**, *27* (34), 5002−5008.

(5) Zhang, L.; Chan, J. M.; Gu, F. X.; Rhee, J.-W.; Wang, A. Z.; Radovic-Moreno, A. F.; Alexis, F.; Langer, R.; Farokhzad, O. C. Self-Assembled Lipid−Polymer Hybrid Nanoparticles: A Robust Drug Delivery Platform. *ACS Nano* **2008**, *2* (8), 1696−1702.

(6) Appel, E. A.; Tibbitt, M. W.; Greer, J. M.; Fenton, O. S.; Kreuels, K.; Anderson, D. G.; Langer, R. Exploiting Electrostatic Interactions in Polymer−Nanoparticle Hydrogels. *ACS Macro Lett.* **2015**, *4* (8), 848−852.

(7) Bongio, M.; van den Beucken, J. J. J. P.; Leeuwenburgh, S. C. G.; Jansen, J. A. Development of bone substitute materials: from 'biocompatible' to 'instructive'. *J. Mater. Chem.* **2010**, *20* (40), 8747−8759.

(8) Sen, M. K.; Miclau, T. Autologous iliac crest bone graft: should it still be the gold standard for treating nonunions? *Injury* **2007**, *38* (1), S75−80.

(9) Willie, B. M.; Petersen, A.; Schmidt-Bleek, K.; Cipitria, A.; Mehta, M.; Strube, P.; Lienau, J.; Wildemann, B.; Fratzl, P.; Duda, G. Designing biomimetic scaffolds for bone regeneration: why aim for a copy of mature tissue properties if nature uses a different approach? *Soft Matter* **2010**, *6* (20), 4976−4987.

(10) Dawson, J. I.; Oreffo, R. O. Bridging the regeneration gap: stem cells, biomaterials and clinical translation in bone tissue engineering. *Arch. Biochem. Biophys.* **2008**, *473* (2), 124−31.

(11) Lutolf, M. P.; Gilbert, P. M.; Blau, H. M. Designing materials to direct stem-cell fate. *Nature* **2009**, *462* (7272), 433−41.

(12) Wong Po Foo, C. T.; Lee, J. S.; Mulyasasmita, W.; Parisi-Amon, A.; Heilshorn, S. C. Two-component protein-engineered physical hydrogels for cell encapsulation. *Proc. Natl. Acad. Sci. U. S. A.* **2009**, *106* (52), 22067−72.

(13) Mulyasasmita, W.; Lee, J. S.; Heilshorn, S. C. Molecular-level engineering of protein physical hydrogels for predictive sol-gel phase behavior. *Biomacromolecules* **2011**, *12* (10), 3406−11.

(14) Goodman, S. B.; Yao, Z.; Keeney, M.; Yang, F. The future of biologic coatings for orthopaedic implants. *Biomaterials* **2013**, *34* (13), 3174−3183.

(15) Luz, G. M.; Mano, J. o. F. Mineralized structures in nature: Examples and inspirations for the design of new composite materials and biomaterials. *Compos. Sci. Technol.* **2010**, *70* (13), 1777−1788.

(16) Albrektsson, T.; Johansson, C. Osteoinduction, osteoconduction and osseointegration. *European spine journal: official publication of the European Spine Society, the European Spinal Deformity Society, and the European Section of the Cervical Spine Research Society* **2001**, *10* (Suppl 2), S96−101.

(17) Alves, N. M.; Leonor, I. B.; Azevedo, H. S.; Reis, R. L.; Mano, J. F. Designing biomaterials based on biomineralization of bone. *J. Mater. Chem.* **2010**, *20* (15), 2911−2921.

(18) Webster, T. J.; Ergun, C.; Doremus, R. H.; Siegel, R. W.; Bizios, R. Enhanced functions of osteoblasts on nanophase ceramics. *Biomaterials* **2000**, *21* (17), 1803−10.

(19) Weiner, S. Biomineralization: a structural perspective. *J. Struct. Biol.* **2008**, *163* (3), 229−34.

(20) Bhumiratana, S.; Grayson, W. L.; Castaneda, A.; Rockwood, D. N.; Gil, E. S.; Kaplan, D. L.; Vunjak-Novakovic, G. Nucleation and growth of mineralized bone matrix on silk-hydroxyapatite composite scaffolds. *Biomaterials* **2011**, *32* (11), 2812−20.

DOI: 10.1021/acsbiomaterials.6b00286
ACS Biomater. Sci. Eng. XXXX, XXX, XXX−XXX

(21) Gaharwar, A. K.; Dammu, S. A.; Canter, J. M.; Wu, C. J.; Schmidt, G. Highly extensible, tough, and elastomeric nanocomposite hydrogels from poly(ethylene glycol) and hydroxyapatite nanoparticles. *Biomacromolecules* **2011**, *12* (5), 1641−50.
(22) Chung, W. J.; Kwon, K. Y.; Song, J.; Lee, S. W. Evolutionary screening of collagen-like peptides that nucleate hydroxyapatite crystals. *Langmuir* **2011**, *27* (12), 7620−8.
(23) Gungormus, M.; Fong, H.; Kim, I. W.; Evans, J. S.; Tamerler, C.; Sarikaya, M. Regulation of in vitro calcium phosphate mineralization by combinatorially selected hydroxyapatite-binding peptides. *Biomacromolecules* **2008**, *9* (3), 966−73.
(24) Roy, M. D.; Stanley, S. K.; Amis, E. J.; Becker, M. L. Identification of a Highly Specific Hydroxyapatite-binding Peptide using Phage Display. *Adv. Mater.* **2008**, *20* (10), 1830−1836.
(25) Parisi-Amon, A.; Mulyasasmita, W.; Chung, C.; Heilshorn, S. C. Protein-engineered injectable hydrogel to improve retention of transplanted adipose-derived stem cells. *Adv. Healthcare Mater.* **2013**, *2* (3), 428−32.
(26) Russ, W. P.; Lowery, D. M.; Mishra, P.; Yaffe, M. B.; Ranganathan, R. Natural-like function in artificial WW domains. *Nature* **2005**, *437* (7058), 579−83.
(27) Weiger, M. C.; Park, J. J.; Roy, M. D.; Stafford, C. M.; Karim, A.; Becker, M. L. Quantification of the binding affinity of a specific hydroxyapatite binding peptide. *Biomaterials* **2010**, *31* (11), 2955−63.
(28) Cowan, C. M.; Shi, Y. Y.; Aalami, O. O.; Chou, Y. F.; Mari, C.; Thomas, R.; Quarto, N.; Contag, C. H.; Wu, B.; Longaker, M. T. Adipose-derived adult stromal cells heal critical-size mouse calvarial defects. *Nat. Biotechnol.* **2004**, *22* (5), 560−7.
(29) Lo, D. D.; Hyun, J. S.; Chung, M. T.; Montoro, D. T.; Zimmermann, A.; Grova, M. M.; Lee, M.; Wan, D. C.; Longaker, M. T., Repair of a critical-sized calvarial defect model using adipose-derived stromal cells harvested from lipoaspirate. *J. Visualized Exp.* **2012**, *68* (68). DOI: 10.3791/4221.
(30) Discher, D. E.; Mooney, D. J.; Zandstra, P. W. Growth factors, matrices, and forces combine and control stem cells. *Science* **2009**, *324* (5935), 1673−7.
(31) Engler, A. J.; Sen, S.; Sweeney, H. L.; Discher, D. E. Matrix elasticity directs stem cell lineage specification. *Cell* **2006**, *126* (4), 677−89.
(32) Huebsch, N.; Lippens, E.; Lee, K.; Mehta, M.; Koshy, S. T.; Darnell, M. C.; Desai, R. M.; Madl, C. M.; Xu, M.; Zhao, X.; Chaudhuri, O.; Verbeke, C.; Kim, W. S.; Alim, K.; Mammoto, A.; Ingber, D. E.; Duda, G. N.; Mooney, D. J. Matrix elasticity of void-forming hydrogels controls transplanted-stem-cell-mediated bone formation. *Nat. Mater.* **2015**, *14* (12), 1269−77.

DOI: 10.1021/acsbiomaterials.6b00286
ACS Biomater. Sci. Eng. XXXX, XXX, XXX−XXX